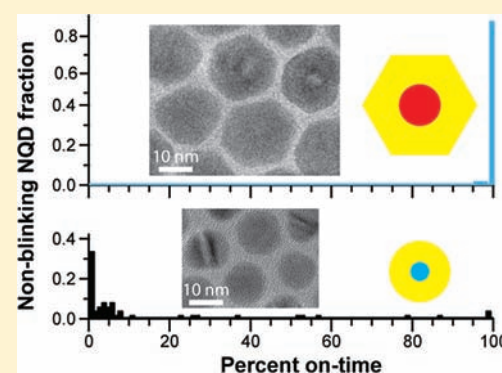# New Insights into the Complexities of Shell Growth and the Strong Influence of Particle Volume in Nonblinking "Giant" Core/Shell Nanocrystal Quantum Dots

Yagnaseni Ghosh,[†] Benjamin D. Mangum,[†] Joanna L. Casson,[‡] Darrick J. Williams,[†] Han Htoon,[†] and Jennifer A. Hollingsworth*,[†]

[†]Materials Physics & Applications Division, Center for Integrated Nanotechnologies and [‡]Chemistry Division, Physical Chemistry & Applied Spectroscopy, Los Alamos National Laboratory, Los Alamos, New Mexico 87545, United States

ⓢ *Supporting Information*

ABSTRACT: The growth of ultra-thick inorganic CdS shells over CdSe nanocrystal quantum dot (NQD) cores gives rise to a distinct class of NQD called the "giant" NQD (g-NQD). g-NQDs are characterized by unique photophysical properties compared to their conventional core/shell NQD counterparts, including suppressed fluorescence intermittency (blinking), photobleaching, and nonradiative Auger recombination. Here, we report new insights into the numerous synthetic conditions that influence the complex process of thick-shell growth. We show the individual and collective effects of multiple reaction parameters (noncoordinating solvent and coordinating-ligand identities and concentrations, precursor/NQD ratios, precursor reaction times, etc.) on determining g-NQD shape and crystalline phase, and the relationship between these structural features and optical properties. We find that hexagonally faceted wurtzite g-NQDs afford the highest ensemble

quantum yields in emission and the most complete suppression of blinking. Significantly, we also reveal a clear correlation between g-NQD particle volume and blinking suppression, such that larger cores afford blinking-suppressed behavior at relatively thinner shells compared to smaller starting core sizes, which require application of thicker shells to realize the same level of blinking suppression. We show that there is a common, threshold g-NQD volume ($\sim$750 nm^3) that is required to observe blinking suppression and that this particle volume corresponds to an NQD radiative lifetime of $\sim$65 ns regardless of starting core size. Combining new understanding of key synthetic parameters with optimized core/shell particle volumes, we demonstrate effectively complete suppression of blinking even for long observation times of $\sim$1 h.

■ INTRODUCTION

So-called "giant" nanocrystal quantum dots (g-NQDs), especially ultra-thick-shell CdSe/CdS core/shell systems (>10 monolayers of CdS),[1,2] have garnered a great deal of attention as a result of their important and unusual photophysical properties. With increasing shell thickness, CdSe/CdS NQDs exhibit increasing degrees of blinking suppression[1−3] and near elimination of nonradiative Auger effects,[4−7] two properties once considered intrinsic to conventional (nonalloyed) core-only or core/shell NQDs. The novel thick-shell CdSe/CdS core/shell systems are also characterized by enhanced chemical and photostability, exhibiting retention of optical properties following ligand exchange and thermal annealing or transfer to aqueous environments, as well as elimination of photobleaching.[1,2] Taken together, these properties have important implications for g-NQDs as single-photon sources, molecular probes for single-particle tracking, and active emitters for low-threshold lasers and robust solid-state lighting.

Despite extensive exploration of g-NQD photophysical properties,[4−7] and even practical demonstrations of their utility in light-emitting devices,[8] relatively less is known about the details of the shell-growth process that leads to these remarkable characteristics. To grow very thick, uniform shells of CdS onto CdSe (lattice mismatch: 3.9%) with retention of crystalline quality and minimal introduction of defects, the Successive Ionic Layer Adsorption and Reaction (SILAR) approach has been used.[1,3] With SILAR, chemists aim to introduce shell material monolayer-by-monolayer by *sequentially* adding monolayer equivalents of cation and anion precursors to NQD cores suspended in a mixture of noncoordinating solvent(s) and coordinating ligand(s).[9,10] Compared to earlier approaches that relied on co-injection of cation and anion precursors at necessarily low temperatures (to avoid homogeneous nucleation of shell material as separate nanoparticles), SILAR offered the advantage of higher shell-growth temperatures. In the case of SILAR, each aliquot of cation precursor introduced to the reaction, for example, was assumed to add to the NQD surface before the subsequent addition of anion precursor took place, affording exclusively

heterogeneous nucleation and growth.[9,10] SILAR is likely not required for growth of thin shells and is perhaps not required in the case of lattice-matched systems; however, this approach was clearly shown to improve the size distribution of moderately thick-shell CdSe/ZnS core/shell NQDs (large lattice match: 12%) compared to their single-injection counterparts.[10] For these reasons, synthesis of thick-shell core/shell NQDs has generally benefited from this more controlled approach. Significantly, SILAR growth proceeds roughly as expected, with the number of predicted shell monolayers (calculated based on the amount of precursor added) generally matching the number of shell monolayers obtained (determined from transmission electron microscopy, TEM, size determinations), even in the case of ultra-thick-shell g-NQDs (>10 shell monolayers).[1] That said, SILAR growth out to such thick shells is complicated by a number of growth parameter variables that are, to date, not sufficiently well understood. Likely for this reason, synthesis of g-NQDs can lead to unwanted variations in optical and structural properties.

Additionally, although much attention has been paid to the effect of shell thickness on thick-shell CdSe/CdS NQD photophysical properties,[1−7] the effect of *core size* remains unexplored in this context. To date, the impact on g-NQD optical properties of tuning core size from very small (~2 nm) to very large (>5 nm) is not known. In the case of CdSe core-only or thin-shell core/shell systems, core size tuning has traditionally been used to achieve emission colors across the visible spectrum (~500−700 nm). However, due to significant red-shifting of spectral emission with increasing shell thickness,[1,3] this degree of color tuning is not expected in the case of CdSe/CdS g-NQDs. Nonetheless, the full range of achievable emission wavelengths remains to be determined. More significantly, it is not currently known whether shell thickness is the exclusive factor underlying the previously observed shell-dependent suppression of blinking. Without an equal analysis of differently sized core systems, it is not possible to distinguish shell-thickness from particle-volume effects, where the latter would necessarily include the contribution of core size.

Here, we provide new insight into the SILAR synthesis of ultra-thick-shell CdSe/CdS g-NQDs. We report a systematic analysis of key reaction parameters and their influence on g-NQD physicochemical and optical (ensemble and single-particle) properties. Lastly, we clearly show that core size—as it contributes to total particle volume—has a strong influence on g-NQD blinking behavior. Finally, by combining a new understanding of the SILAR growth process for thick-shell NQD systems with large NQD core/shell particle volumes (>750 nm³), we show for the first time that CdSe/CdS g-NQDs can provide complete suppression of blinking.

■ MATERIALS AND METHODS

Materials. Cadmium oxide (CdO, 99.95%), oleic acid (90%), 1-octadecene (ODE, 90%), 1-octadecane (OD, 90%) oleylamine (tech grade), sulfur powder (99.98%), selenium pellet (≥99.999%), and trioctyl phosphine (TOP) (97%) were purchased from Aldrich and used without further purification. Trioctyl phosphine oxide (TOPO) (90%) was purchased from Strem and used without further purification.

General Methods. Absorption and emission spectra were recorded using a CARY UV-Vis-NIR spectrophotometer and a Horiba NanoLog spectrofluorometer, respectively. Fourier transform infrared spectroscopy (FTIR) was conducted using a Nicolet 6700 spectrometer. Samples for FTIR were prepared by placing a drop of rigorously purified (six precipitation/resuspension washing cycles to remove unbound oleic acid/oleate and amines) NQD solution on the surface of a diamond attenuated total reflectance (ATR) FTIR cell. After the solvent evaporated, FTIR spectra were collected using 4 cm⁻¹ resolution, with 32 scans being accumulated for statistical averaging. FTIR spectra of pure oleic acid, oleyl amine, dioctylamine, trioctylphosphine, and trioctylphosphine oxide were obtained by similar analysis of samples cast from hexane−surfactant solutions onto the diamond ATR cell. Transmission electron microscopy (TEM) images were obtained using a JEOL 2010 transmission electron microscope. Powder X-ray diffraction patterns were obtained using a Rigaku Ultima III diffractometer that employs a Cu Kα (λ = 1.5406 Å) X-ray source. XRD samples were deposited onto a background-less silicon slide. Data were collected in continuous scan mode in parallel beam slit geometry over the 2θ range from 10 to 90° with sampling width of 0.005° and a scanning speed of 0.100°/min.

Single-NQD Imaging. NQD samples were diluted in hexane and drop-cast onto acetone cleaned glass coverslips. The dilution factor was changed until single NQDs were well resolved. These samples were excited using a continuous wave laser diode operating at 405 nm (Coherent Cube). An average power of ~15 mW was focused using a simple lens such that the roughly circular focal spot achieved a diameter of ~75 μm. Single NQD PL was collected with a microscope objective and focused onto a liquid nitrogen cooled CCD detector (Princeton Instruments Spec-10). The PL was directed through both a dichroic mirror and a spectral filter to reject excitation light and reduce background noise. A time series of 20 000 image frames were collected with an integration time of 100 ms with a delay of ~90 ms readout time between saved image frames. In this manner, the total acquisition time is slightly longer than 1 h, the sample being under constant illumination. A custom-written computer program (operating in Igor Pro) was used to determine the grouping of pixels that constitute a single dot, and consequently find each dot's intensity level for each of the image frames. The average background intensity for each frame was also determined. The threshold for describing an NQD as "on" was related to the background level as follows:

$$I_{pix} > BG + 2\sqrt{BG} \Rightarrow ON$$

where I_{pix} is the average intensity per pixel per dot and BG is the background counts per pixel. Note that even when the single dot fails to meet the above criteria and is technically considered to be in an off state, the image of that particular dot can often still be discerned. Also note that in calculating I_{pix}, no background subtraction has been performed. Each dot is subsequently given a binary value and blinking statistics are calculated as the number of dots in an on state compared to the total number of dots that ever emitted light during the 1 h measurement time.

Lifetime Measurements. NQD dispersions in hexane were drop-cast onto acetone cleaned glass coverslips forming a rough film. A ~70 ps pulsed laser diode operating at 405 nm (PicoQuant LDH-P-C-405B) was used to excite the samples, at repetition rates between 400 kHz and 2.5 MHz. The samples were excited under wide-field illumination (~100 μm diameter spot) with the average laser power attenuated using neutral density filters (typically in the range of several nW to hundreds of pW), which corresponds to an average number of excitons per dot per pulse of $\langle N \rangle \approx 10^{-5}$. PL was collected with a 100×, 1.3 NA oil immersion microscope objective and directed through both a dichroic mirror and a long pass filter to exclude any excitation light. Ultimately, the PL was focused onto a single photon sensitive avalanche photodiode (Perkin-Elmer SPCM-AQR-14), where the arrival times of individual photons were subsequently recorded using a time-correlated single photon counting system (PicoQuant PicoHarp 300). Lifetimes were built up by making histograms of photon arrival times and analyzed by curve fitting using Igor Pro. Tri-exponential curves were fit to each lifetime histogram. Lifetime values reported here are average lifetimes defined in the following manner:[11]

$$T_{avg} = \sum_m \frac{a_m T_m^2}{\sum_n a_n T_n}$$

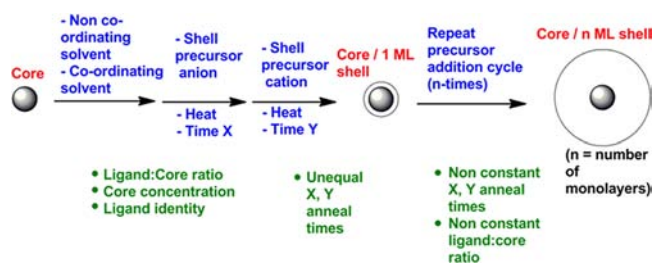where a and T represent the amplitude and lifetime coefficients of the fit.

Optimized Synthetic Protocol for g-NQDs. *CdSe Core Synthesis.* The CdSe core was prepared by reported procedure[4] with minor modifications. A 100 mL round-bottom (r.b.) flask equipped with a reflux condenser and a thermocouple probe was charged with 1 g of TOPO, 8 mL of ODE, and 0.38 mmol of Cd−oleate under standard air free conditions. The reaction system was evacuated for 30 min at room temperature and 30 min at 80 °C, and then the temperature was raised to 300 °C under Argon, following which a mixture of 4 mmol of TOP−Se, 3 mL of oleylamine, and 1 mL of ODE was quickly injected into the reaction system. The temperature was then lowered to 270 °C for CdSe NQD growth. After several minutes, the solution was cooled down to room temperature, and CdSe NQDs (diameter, d, = 3 or 4 nm) were collected by precipitation with ethanol and centrifugation. CdSe NQDs were redispersed in hexane after 2−3 cycles of precipitation/ collection. To obtain ultra-small cores (d = 2.2 nm), growth was arrested by adding cold toluene to the reaction flask several seconds after the Se injection. To obtain extra-large cores (d = 5.5 nm), the initial growth was allowed to proceed for ∼10 min, after which additional precursor (0.8 mmol Cd−oleate and 8 mmol TOP−Se) was added dropwise at 270 °C, followed by an additional 10 min growth at 300 °C.

CdSe/nCdS Core−Shell g-NQD Synthesis. The synthesis of core− shell CdSe/nCdS g-NQDs followed the familiar SILAR approach pioneered by Peng and co-workers[9] with fine-tuned modifications. A 250 mL r.b. flask was charged with ∼2 × 10^{-7} mol of washed CdSe cores, 5 mL of oleylamine, and 5 mL of OD. Here, OD was specifically chosen as the solvent as it alleviated the problem of precipitation observed during later stages of thick shell growth (see Results and Discussion). Stock solutions of 0.2 M elemental sulfur dissolved in OD and 0.2 M Cd−oleate in OD were used as precursors for shell growth. Before beginning SILAR, the Se-rich surfaces of the CdSe cores were passivated by addition of Cd−oleate equivalent to one monolayer of Cd. The quantity of precursors for growing each monolayer of shell was calculated according to the volume increment of each monolayer shell, considering the changing total NQD size with each successive monolayer grown. For the first 5−8 shell−monolayer deposition cycles, the Cd/oleic acid ratio in the 0.2 M Cd−oleate stock solution was 1:4, while that for the stock solution used for each succeeding layer was 1:10. The reaction temperature was set at 240 °C. Growth times were 1 h following each sulfur addition and 2.5 h following each cadmium addition. Reactions were continued until desired shell thickness was achieved. Following each complete shell-monolayer addition cycle, 1% of the total volume of the reaction solution was withdrawn; however, the quantities of added shell precursors were not adjusted to take into account the lesser amount of remaining NQDs, resulting in a shell-precursor excess throughout the shell addition process. g-NQDs were washed by precipitating 2−3 times with ethanol and redispersing in hexane. Relative quantum yields (QYs) in emission were determined in comparison to a standard dye (Rhodamine 6G, 99%, Acros) and were observed to vary as a function of shell thickness.

■ RESULTS AND DISCUSSION

Scheme 1 shows the basic flow of the SILAR approach to synthesis of core/shell NQDs. It also reveals the complex array of reaction parameters that can influence the process of shell addition. For growth of conventional thin-shell NQDs (approximately 1−3 monolayers of shell material), the exact choice and implementation of these parameters may not significantly affect the outcome of the shell addition procedure. In contrast, these variables can dramatically affect the resulting structural and functional characteristics of thick-shell NQDs. Here, we investigate multiple key growth parameters and correlate each with changes to NQD structure (shape and crystalline phase) and optical properties (ensemble QYs, emission lifetimes, and single-NQD level blinking).

Scheme 1. SILAR Reaction Scheme for Growth of Thick-Shell Core/Shell NQDs[a]

[a]Blue text denotes general reaction parameters and reaction flow, while green text shows options for modifying specific reaction conditions to influence g-NQD physicochemical and optical properties.
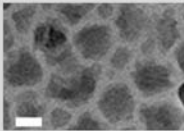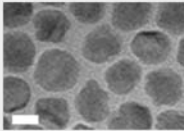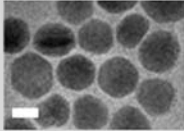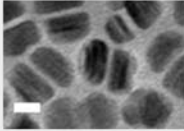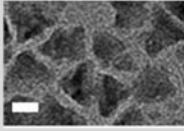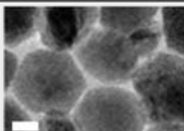
The originally reported SILAR method for growing core/ shell NQDs[9] utilized short anneal times following each addition of precursor material. For example, in the case of SILAR growth of ZnS shell onto CdSe cores, between each addition of shell precursor (Zn or S), the system was allowed to equilibrate for 10 min. This "reaction" or "anneal" time was deemed sufficient to permit complete incorporation of the respective half monolayer of Zn or S. Indeed, we observe that such rapid addition of shell monolayers (in our case, CdS monolayers) does roughly produce the correct core/shell "size," even in the case of thick-shell systems. The core/shell NQD sizes determined by transmission electron microscopy (TEM) correlate well with theoretical values calculated using the known core size and assumed shell thicknesses (one monolayer, ML, = 0.3375 nm) (Supporting Information, Figure S1).

Importantly, however, we observe that longer anneal times afford improved ensemble optical properties in both moderate (≥5 ML) and thick-shell regimes. QYs in emission for CdSe cores (obtained after at least two precipitation and washing steps) are typically 15−20%, and application of a thin CdS shell results in large enhancements (3−4-fold), independent of anneal times. This is not the case for thicker shell (11 and 15 ML) systems, where well-defined correlations are observed. In these cases, shell-growth or anneal times exert a significant and consistent effect on QYs (Table 1). For identical cores and otherwise equivalent growth parameters, shorter reaction times allotted for per-monolayer shell growth result in lower emission

Table 1. Influence of Shell-Addition Anneal Protocol on Core/Shell Ensemble NQD Optical Properties

Anneal times	Quantum Yields in Emission (%)		
	At 5 MLs	At 11 MLs	At 15 MLs
Post S: 10 min Post Cd: 10 min	∼20	∼10	∼5
Post S: 10 min Post Cd: 3 h	>45	∼40	∼15
Post S: 3 h Post Cd: 10 min	∼35	∼10	∼6
Post S: 1 h Post Cd: 3 h	∼70	∼25	∼20
Post S: 3 h Post Cd: 1 h	∼25	∼10	∼5

Table 2. Influence of Noncoordinating Solvent and Coordinating Ligand Parameters on Solubility Cycling and Core/Shell Structural and Optical Properties

Solvent / Ligand Variables	Onset of Precipitation	Shape	Wurtzite: Zinc-Blende Ratio	QY at thickest shells (>15 ML)	TEM images (scale bar equals 10 nm)
Octadecene / Primary Amine	Early	Rounded at thin shells, but polydisperse at thick shells	80:20	Low	
Octadecane / Primary Amine	Middle	Improved structural dispersity	74:26	Low	
Octadecane / Primary Amine (longer anneal times)	Middle to late	Rounded to faceted hexagonal (>15 MLs)	~85:15	Mod-High	
Octadecane / Primary Amine (extreme dilution)	None	Half-moons	60:40	Low	
Octadecane / Secondary Amine	None	Octahedral	~70:30	None	
Octadecane / No Added Amine	Early	Faceted hexagonal (>6 MLs)	~80:20	Mod-High	

efficiencies compared to longer times. Specifically, growth times of 20 min (10 min following Cd addition and 10 min following S addition) produce average QYs of 21 ± 0.2% after addition of 5 shell monolayers. In contrast, total shell growth times of 3 h for the same CdSe core material result in an average QY of 41 ± 6% after application of 5 shell monolayers.

The larger variation (±6%) in this latter QY results from our averaging of values obtained for reactions employing the same total shell monolayer growth times, but *different relative growth times* for the cation and anion precursors. Relatively longer pause, or anneal, times after Cd addition and shorter pause times after S addition result in higher QYs for CdSe/5 ML-CdS NQDs. In this case, by waiting ~3 h following cadmium addition before subsequent sulfur addition, and only 10 min between sulfur addition and the next cadmium addition, we obtained QYs that were >45% compared to ~35% in the opposite case (10 min pause between cadmium and subsequent sulfur addition and ~3 h pause after addition of sulfur). Similar relative differences were also observed in the case of a 4 h total anneal time, and this trend, in all instances, continued for thicker shell systems (Table 1).

In summary, long total per-monolayer growth (anneal) times are optimal for enhancing QYs for both moderate (≥5 ML) and thicker shell systems This result is not obvious from studying thin-shell systems alone. Also, an asymmetric distribution of anneal times between cadmium and sulfur

precursors results in improvements in QY, where relatively longer anneal times following cadmium precursor addition are favored. That said, thick-shell g-NQD ensemble QYs still suffer from batch-to-batch variability, more-so compared to their thin-shell counterparts, and are in general unacceptably low for any application that would demand near-unity QYs (e.g., replacement down-conversion phosphors in solid-state lighting).[12]

Although QYs as high as 40% are possible in the case of the thickest-shell systems (11−20 ML) using our previously reported protocol,[1] lower values (≤25%) are more regularly obtained. Interestingly, even though single-g-NQD optical properties have continued to improve, namely, nonblinking fractions (defined as: fraction of g-NQD population "on" for >99% of the total observation time of 60 min) have increased from 20%[1] to 50%,[2] and, here, to >85% (see below), ensemble-level QYs have not been so dramatically enhanced to date. For this reason, we explore reaction parameters beyond growth times to effect more global optimization of g-NQD properties.

"Solubility Cycling" during Thick-Shell Growth: Impact of Noncoordinating Solvent and Coordinating Ligands. We have observed that at some point during the thick-shell-addition process, CdSe/CdS core/shell NQDs precipitate from their reaction solution. Such precipitation generally occurs after 7 shell monolayers have been added to 3−4 nm CdSe cores. Specifically, the addition of cadmium

precursor solution (cadmium oleate in oleic acid) at this stage in the shell-growth cycle causes the reaction mixture to become turbid, while subsequent addition of the sulfur precursor solution (sulfur in octadecene, ODE) results in a return to optical clarity and complete solubilization of the NQDs. For the first several shelling cycles after turbidity is initially observed, only a few drops of the sulfur solution are required to effect redissolution of the particle slurry. The process behaves as a titration reaction, as each successive drop of sulfur in ODE results in increasing clarity of the reaction solution. At higher shell monolayers (>11 ML), however, addition of even the entire sulfur aliquot does not eliminate the turbidity.

The degree of reaction homogeneity or inhomogeneity is an important reaction criterion, as it influences the processes by which cadmium and sulfur adatoms interact with the NQD surface. Specifically, interfacial processes of atom adsorption–desorption and surface migration permit atoms initially located at nonlattice sites on the surface of a growing crystal—here, the surface of the core/shell NQD—to relocate to regular crystal lattice positions. These processes are critical for obtaining high-quality, crystalline NQDs with minimal incorporation of defects. They are well supported in a homogeneous reaction solution that affords efficient reactant transfer between the NQD surface and the solvent phase, where the presence of coordinating ligands serves both to passivate surface-bound atoms and to provide a means for atom exchange with the solution by stabilizing solution-phase ions. In contrast, inhomogenous environments resulting from fluctuations in particle solubility likely lead to within-batch and batch-to-batch variability in g-NQD structural and optical properties. Indeed, as-prepared thick-shell g-NQDs can often exhibit significant morphological variations in a single reaction product (Table 2, Data Row 1). To minimize within-batch and batch-to-batch variability possibly resulting from the observed precipitation process, we modified several reaction parameters expected to influence particle stability in solution.

Surprisingly, merely replacing ODE with octadecane (OD) resulted in a dramatic change in the onset of turbidity. With OD, initial onset of turbidity was delayed until at least 11 shell monolayers, compared to precipitation occurring as early as 7 shell monolayers in the case of ODE. Also, limited dilution with OD at later stages of growth (starting at 10 shell monolayers: NQD concentration reduced from 9×10^{-6} to 7×10^{-6} M) further suppressed precipitation and resulted in improvements in g-NQD size and shape uniformity (Table 2, Data Row 2). Combined with longer per-monolayer growth times (as described above), these modified reaction conditions afforded highly symmetric, spherical g-NQDs (Table 2, Data Row 3). It should be noted, however, that "extreme" dilution of the CdSe NQD cores (to 1.5×10^{-6} M) at the start of the shelling process was counterproductive. Although turbidity was entirely eliminated, the product was characterized by unusual 'half-moon'-shapes (Table 2, Data Row 4), polytypic crystal structure, and low PL QYs at all shell thicknesses (<15%).

We also explored the effect of coordinating ligands on the progression of shell growth. For a typical shell addition process, we employed a combination of a primary amine (oleylamine) and oleic acid. The amine (15 mmol) is added in its entirety at the beginning of the reaction, while oleic acid (OA) is added with each aliquot of cadmium precursor in a ratio of 1:4 or 1:10 Cd/OA. The amine can serve both as a coordinating ligand and as a base to deprotonate oleic acid to form oleate, where the reaction medium is postulated to be sufficiently polar to

stabilize the resulting ionic species. (By mass, the reaction medium comprises an approximately equal mixture of nonpolar OD or ODE and polar oleic acid/oleylamine.) Oleate then covalently binds to surface Cd ions, while oleylamine datively couples to Cd. The extent to which the amine serves as a coordinating ligand appears to be determined by the amount of oleic acid (oleate) present in the reaction. When less oleic acid is added to the reaction with each addition of cadmium precursor (1:4 Cd/OA), amines dominate the FTIR spectra of thick-shell NQDs (Figure 1a,d), as evidenced from the
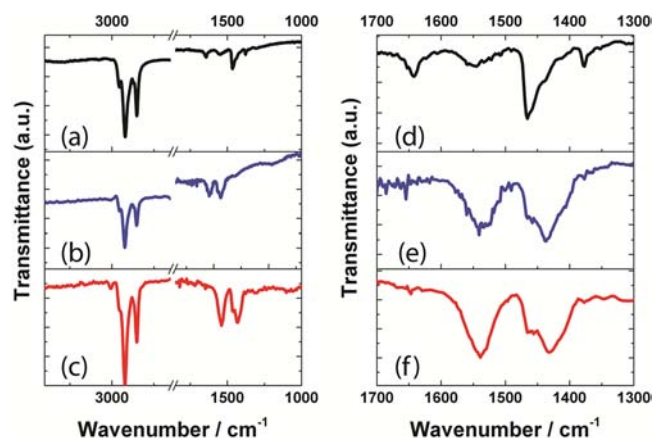

Figure 1. FTIR spectra of core/shell NQDs synthesized using different ligands and/or ligand/precursor ratios. (a−c) Full FTIR spectra from 3500 to 1000 cm^{-1}, where the characteristic stretches from 2950 to 2850 cm^{-1} correspond to −CH$_3$ and −CH$_2$ functional groups of the oleyl moiety. (d−f) Signature region (1700−1300 cm^{-1}) for −NH$_2$ and −COO$^-$ functional groups. (a and d) Primary amine and 1:4 Cd/oleate in growth mixture leads to a mixture of amine (δ(NH$_2$) bending mode at ~1635 cm^{-1}) and oleate (ν_{as}(COO$^-$) and ν_s(COO$^-$) stretching modes at 1555 and 1408 cm^{-1}) surface-capping ligands. (b and e) Primary amine and 1:10 Cd/oleate in growth mixture leads to exclusively oleate capping of the g-NQDs. (c and f) Secondary amine and 1:4 Cd/oleate in growth mixture also leads to exclusively oleate capping.

(δ(NH$_2$) bending mode at ~1635 cm^{-1}. In contrast, higher OA amounts (1:10 Cd/OA) result in oleate dominating ligand coverage at thicker shells (Figure 1b,e). Note: signatures of oleic acid (−C≡O stretching mode that appears around 1710 cm^{-1}), as opposed to oleate [ν_{as}(COO$^-$) and ν_s(COO$^-$) stretching modes at 1555 and 1408 cm^{-1}], are rarely observed in our FTIR studies of core/shell NQD surfaces (Supporting Information, Figure S2). This suggests that the presence of an excess of amine (15 mmol amine vs 6.5 mmol OA after 14 shell-monolayers have been added) affords sufficient conversion of oleic acid to the anionic oleate to allow this more reactive species to effectively outcompete its protonated (acid) counterpart in binding to NQD surfaces. Interestingly, the oleate-coated particles (reaction Cd/OA ratio = 1:10) are relatively more faceted than the amine-coated particles (reaction Cd/OA ratio = 1:4), which appear more rounded (Supporting Information, Figure S3). In both cases, however, moderate to high QYs can be obtained, and XRD analysis indicates predominantly wurtzite crystal structures (Table 2, Data Row 3, average values shown).

Replacing the primary amine ligand (oleylamine) with a secondary amine (dioctylamine) has a dramatic effect on the progression of the reaction. In this case, precipitation during shell growth is completely eliminated. This apparent improve-

ment in reaction homogeneity does not translate into improved optical properties, however, as the resulting NQDs are nonemissive. Intriguingly, these particles exhibit an octahedral shape (Table 2, Data Row 5), though a predominantly wurtzite phase (Supporting Information, Figure S4). Such a structure has been described previously for CdSe NQDs[13] and is characterized by 8 (4 forming the top hemisphere and 4 forming the bottom hemisphere) alternating $\pm(0001)$ (all-Cd or all-S) facets. Unlike hexagonal NQDs, which are inherently anisotropic due to their being terminated on one end by a (0001) face (all-Cd) and on the other by a $(000\bar{1})$ face (all-S), octahedral NQDs should be overall "nonpolar" (see below: Solubility-Cycling Mechanism discussion). Each Cd face is balanced both laterally and axially by an S face. The thick-shell NQDs produced in the presence of dioctylamine were found to be exclusively oleate capped (Figure 1c,f), even when lesser oleic acid was used in the reaction (1:4 Cd/OA). This is in contrast with an otherwise equivalent primary amine reaction. We explain such an observation by speculating that the secondary amine can serve effectively as a base to produce oleate, but its role as a ligand is compromised by its relatively greater steric bulk compared to oleylamine, which limits its ability to compete with oleate for NQD surface sites. Such steric effects on ligand coverage are likely especially relevant in the case of thick-shell NQDs, as thinner shell NQDs extracted from these reactions do show dioctylamine signatures in their FTIR spectra (Supporting Information, Figure S6). The absence of the sterically more bulky dioctylamine on the thick-shell NQDs presumably results from the progressive "flattening" of the NQD surface with increasing particle size. As surface curvature decreases, ligand end-group crowding is enhanced (Supporting Information, Figure S5). Lastly, since dioctylamine appears to play a relatively minor role as a coordinating ligand, oleate−surface interactions are exclusively responsible for the observed octahedral shape. The ability of oleate to form strong covalent bonds with Cd appears to favor the formation of this unusual particle shape that exposes multiple (4) Cd-terminated faces.

In the case of the primary-amine/oleic acid system that employed significant excess of oleic acid (Cd/OA 1:10), mostly oleate was observed in FTIR at thicker shells, and the faceted hexagonal structure was the principal shape obtained. In contrast, in the case of the primary-amine/oleic acid system that employed less oleic acid (Cd/OA 1:4), both amine and oleate signatures were observed in FTIR at thicker shells (Figure 1a,d), and the particle shapes were rounder and less faceted. It is likely that the surface-reconstructed round particles display less pure-Cd surfaces, minimizing surface energy by distorting the parent hexagonal structure. Here, amines, which form weaker (dative) bonds with Cd, dominate the FTIR spectra, while oleate has a clear presence when the particles are faceted and the all-Cd faces are presumably present.

Eliminating amine from the reaction mixture all together (with the exception of any primary amine remaining from core synthesis bound to the NQD cores) results in the earliest precipitation (from 3 MLs shell onward). Significantly, the NQDs are characterized by hexagonal faceting after fewer shell addition cycles (Table 2, Data Row 6). The fact that this case of extreme oleic-acid dominance correlates with early faceting further supports our assertion that oleic acid (oleate, limited here by the limited supply of amine) favors particle shapes that present all-Cd faces. Also, comparing the onset of precipitation
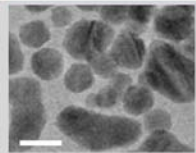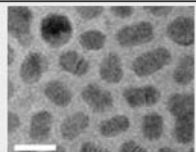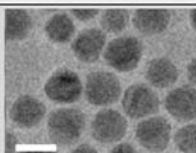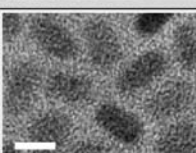
for the different ligand systems, it reveals a relationship between faceting and the precipitation process (see below).

Impact of Reaction Stoichiometry on "Solubility Cycling," and Core/Shell Morphology and Optical Properties. Generally, SILAR shelling protocols employ addition of stoichiometric amounts of precursor. The number of core NQDs present in a reaction is determined (Experimental), and the amount of anion and cation required to grow exactly one monolayer of shell material is calculated based on this NQD-core concentration, as well as the size of the cores. The effective "core" size increases with each addition of a shell layer, requiring increasing amounts of per-monolayer shell precursors as the reaction proceeds. A 100% conversion of the shell precursors is assumed and largely borne out by the observation that core/shell particle sizes determined by TEM are close to that calculated based on the known starting CdSe core size and the thickness of a monolayer of CdS (1/2 wurtzite c lattice parameter: 0.3375 nm).

That said, we questioned whether a strictly stoichiometric shell-precursor/NQD ratio was necessarily optimal. Might not an excess of feedstock better support the dynamic equilibrium of adatom addition, redissolution, and rearrangement that occurs at the solvent/NQD interface? Less "starved" for Cd and/or S atoms, shell growth might be expected to achieve the most stable thermodynamic structure with minimal defects. Indeed, ultradilution, which effectively isolated NQD "cores" from the shell precursor atoms was observed to produce highly defective, nonthermodynamic core/shell particle morphology and crystal structure (Table 2, above). To realize an enhanced shell-precursor/NQD ratio, we systematically removed aliquots from the reaction mixture after each complete shell addition cycle, while maintaining shell precursor quantities at the calculated levels. We extracted aliquots that amounted to 1% and 10% of the reaction volume at each stage of the shelling process. We found that in both cases, post-Cd-addition precipitation at thicker shells was diminished compared to stoichiometric reactions (almost eliminated when 10%-by-volume aliquots were employed). However, QYs were very poor (<10%) for the highest shell-precursor/NQD ratio, and particle morphologies were nonspherical for both (Table 3, Data Rows 1 and 2; note: in this table, TEM images represent moderately thick shell systems as image quality was superior compared to the thickest shell variants). Although emission efficiencies were reasonably high (35−40%) when lesser volume aliquots were removed, rod-like and irregularly shaped particles were formed (Table 3, Data Row 2). Interestingly, however, by combining removal of 1%-volume aliquots with the addition of a small "excess" of oleic acid (2.5 times more oleic acid was added each shell layer starting at the fifth to the eighth shell), high QYs (50%) and symmetric (spherical/hexagonal) morphologies could be maintained out to thick shells (Table 3, Data Row 3), though post-Cd precipitation returned. As previously, increasing the oleic acid concentration results in more "precipitation," but the ensemble structural and optical properties (QYs) reflected the thermodynamic phase (wurtzite) and were improved, respectively (Table 3).

We also attempted a more extreme modification of SILAR protocol. As addition of sulfur precursor was observed to eliminate or reduce the observed turbidity, we attempted to control the precipitation process by supplying the reaction at the start of the shelling process with sulfur precursor sufficient to grow 13 shell monolayers, so that only cadmium precursor was added "monolayer-by-monolayer" (annealing 4 h in

Table 3. Influence of Reaction Stoichiometry on Solubility Cycling, and Core/Shell Structural and Optical Properties

Reaction Stoichiometry Variations	Onset of Precipitation	Shape	QY at thickest shells (>15 ML)	TEM images (scale bar equals 10 nm)
Excess Precursor (10%)	~None	Misshapen	Low	
Excess Precursor (1%)	Late	Rods	Mod.	
Excess Precursor (1%) + Excess Oleic Acid	Middle	Spherical / hexagonal	High	
Constant Sulfur	Middle (minimal & persistent)	Rods	Low	

between each addition of cadmium). Interestingly, this modified SILAR approach did not completely suppress the precipitation process. Turbidity was still observed starting at 7 shell monolayers, but the "solubility cycling" was absent. Instead, an approximately constant and relatively lesser turbidity persisted throughout the shelling process. Despite improvements in overall reaction consistency over time, however, this approach did not produce improved product. The resulting QYs were low. The core/shell NQDs here were predominantly rod-shaped (Table 3, Data Row 4) and characterized by the zinc-blende crystal structure, where wurtzite/zinc-blende ratio from XRD analysis was 40:60 (Supporting Information, Figure S4). This combination of kinetic shape (as compared to isotropic spherical or faceted hexagonal) and phase (as compared to wurtzite, the commonly observed phase for thick-shell CdSe/CdS core/shell NQDs) manifests early in the shell addition process and may result from excess sulfur being present at almost all stages of the reaction. Increased reactant availability is known to facilitate a transition to kinetic growth in the case of elongated NQDs.[14,15] Here, though, the core NQD is spherical, and it is shell growth that is modified by manipulating precursor availability.

"Solubility Cycling": Mechanism and Significance. What triggers the loss of solution-phase stability when the Cd precursor is added and the subsequent return to solution clarity upon S addition? We hypothesize that the S-titratable destabilization is mediated by strong dipole−dipole coupling. Wurtzite CdSe NQDs are characterized by a size-dependent permanent dipole moment that is partially screened by their passivating ligand layer and is also reduced (significantly, nearly an order of magnitude) by surface reconstruction and relaxation.[16] For faceted CdSe NQDs, the different wurtzite

crystal faces are distinct, with unreconstructed (0001) and (000 $\bar{1}$) surfaces comprising all Cd or all S atoms, respectively, while other faces feature mixtures of the anion and cation species.[17] CdSe/CdS NQDs are also characterized by a wurtzite crystal structure, unless prompted toward zinc-blende or polytypic phases by certain modifications of the reaction conditions (as described above). Furthermore, they exhibit clear hexagonal faceting in the case of thicker shell systems (larger overall particle sizes) and/or oleic-acid dominated preparations (as described above).

We surmise that, like their pure CdSe counterparts, CdSe/CdS core/shell NQDs experience an increasing dipole moment as particles are made successively larger by each addition of a CdS shell monolayer, with further enhancements in dipole strength afforded by increased hexagonal faceting. Larger dipole moments translate to intensified NQD−NQD attractive forces along the c-axis that result in particle assembly and solution turbidity. This process is presumably similar to that leading to nanoparticle oriented attachment.[18−20] In fact, we observe evidence of permanent attachment in TEM images. While a majority of the core/shell particles are unattached and, as expected, separated by the ligand layer that coats each particle, some appear as a chain without any intervening ligands (Figure 2). This suggests that for most particles, solution-phase
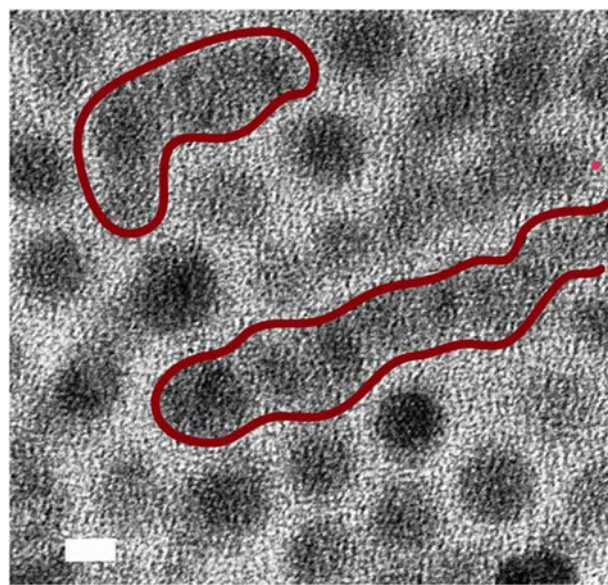

Figure 2. TEM image of CdSe/CdS core/shell NQDs exhibiting dipole−dipole induced particle attachments. Red lines emphasize regions of connected NQDs. Scale bar = 5 nm.

association is temporary/dynamic, but for some, neighboring particles grow together. The instances of attached particles appearing in TEM images are more prevalent for reactions that exhibited the earliest onset of precipitation, that is, the earliest transition from spherical to hexagonal faceting.

That said, it has been speculated that the large dipole moment observed for CdSe NQDs is a feature of all nonmetal nanoparticles, resulting predominantly not from the asymmetric wurtzite crystal structure, but, rather, from the presence of surface localized charges.[21] Surface charges are thought to be present in NQDs as a result of thermally induced charging,[21] even in nonpolar solvents.[22] The observation that cubic zinc-blende ZnSe NQDs possess significant polar character in the

absence of an asymmetric internal lattice symmetry has been cited as evidence for an alternative source of the dipole moment in semiconductor nanocrystals.[21] Interestingly, however, we observe that thick-shell zinc-blende or zinc-blende-dominated CdSe/CdS NQDs, or hexagonal CdSe/CdS NQDs that adopt a more conventionally cubic shape (octahedral; Table 2), do *not* aggregate during the shell-addition process. It, therefore, seems more reasonable to suggest that the wurtzite crystal structure and the resulting hexagonal NQDs possess a strong dipole as a result of the polar nature of the combination of phase and shape that is absent when the particles are polytypic or adopt unusual shapes.

Lastly, the question remains as to why particle association cycles with precursor additions, that is, why does Cd addition effect particle association, while S addition reverses it? Here, we note that only Cd-binding ligands are utilized in the shell addition process. This means that upon addition to the nanocrystal surface, Cd can occupy standard wurtzite lattice sites, terminating dangling bonds with oleate or amine ligands. In contrast, addition of the S atoms, which do not benefit from significant or any ligand stabilization, may lead to surface reconstruction whereby local crystal geometry is altered to maximize bonding and minimize dangling bonds.[16] In this case, the destabilization−restabilization cycles can be viewed as resulting from changes in dipole moment caused by fluctuations in the degree of surface relaxation, where oleate-passivated Cd atoms trend the structure to a more purely wurtzite crystal lattice (larger dipole moment), while S addition promotes surface reconstruction (diminished particle dipole moment). Significantly, this trend is independent of whether we start our shell addition cycles with Cd or S.

Larger Core Sizes Induce Earlier Onset of Blinking Suppression: Nonblinking Fraction Trends with Particle Volume. Previously, we described the effect of increasing CdS shell thickness on blinking suppression for same-size CdSe cores (3.8 nm).[2] Even for these unoptimized thick-shell NQDs, we demonstrated a clear correlation between increasing shell thickness and blinking, improving blinking suppression to the point where nearly half of the g-NQD population was "on" for ≥99% of the unusually long observation time of ∼1 h. The protocol development described here for thick-shell CdSe/CdS NQDs (>10 MLs CdS) has established modified reaction conditions that afford enhanced ensemble optical properties (QYs consistently >50% for the thickest shell systems, i.e., >15 MLs CdS) combined with controlled structural properties, including better particle size and shape uniformity within and across batches. It has also provided a new understanding of the effects of modifying reaction parameters on shape/size-induced "precipitation" cycling during shell growth. A question remains, however, as to how these modifications affect *single-NQD level* optical properties, namely, blinking behavior. In addition, are there any other important parameters to consider in establishing a more definitive understanding of growth-structure−function relationships in the thick-shell CdSe/CdS NQD materials system? Thus far, we have focused on a limited range of core sizes (∼3−4, ∼3.8 nm).[1,2] Now, using our preferred protocol (Experimental), we assess the effect of core size (from 2.2 to 5.5 nm) on blinking suppression.

We find that for each core size the "nonblinking" NQD fraction increases as a function of shell thickness (Figure 3a). However, the onset of blinking-suppression begins at different shell thicknesses for different core sizes: the largest cores exhibit the earliest onset of nonblinking behavior, while the
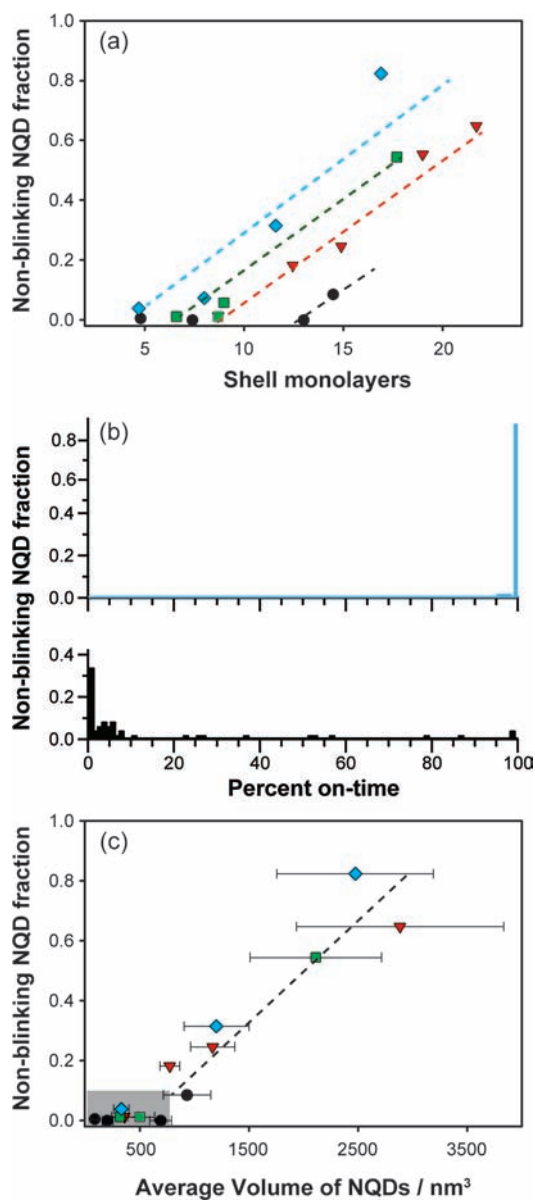

Figure 3. (a) Nonblinking NQD fraction (population of NQDs "on" for ≥99% of the observation time) as a function of shell thickness for different core sizes: black = small core (*d* = 2.2 nm), red = medium core (*d* = 3.0 nm), green = large core (*d* = 4.0 nm), and blue = extra large core (*d* = 5.5 nm). (b) Histogram of blinking statistics for thick-shell NQDs fabricated using an extra-large (top) or a small (bottom) CdSe core. (c) Nonblinking NQD fraction as a function of total particle volume for different starting core sizes; shaded region highlights the particle volumes that fall below the "threshold volume" of ∼750 nm³, above which nonblinking fraction increases approximately linearly with NQD volume.

smallest cores reach this transition at significantly thicker shells. This trend results in the largest cores achieving essentially fully suppressed blinking at thick shells (>85% of the NQDs are nonblinking), while the smallest cores exhibit relatively little nonblinking behavior even after addition of ultra-thick CdS shells (Figure 3b). (Note: though not plotted here, thick-shell NQDs synthesized from larger cores afford hexagonal faceting, more so compared to their small-core counterparts, again implying a correlation between particle shape and optimized optical properties.) Furthermore, plotting nonblinking NQD

fraction as a function of NQD volume (Figure 3c), we find that the combined effects of core size and shell thickness observed in Figure 3a can be understood as a dependency of blinking behavior on *particle volume*. Nonblinking fraction is observed to trend explicitly with core/shell NQD volume, and a clear volume threshold is evident, below which blinking is not suppressed and above which the nonblinking fraction increases roughly linearly with volume. Whether achieved by a combination of a small core and a thick shell or a large core and a relatively thinner shell, the core/shell NQD volume of ~ 750 nm^3 appears to be the minimum volume required for transitioning to nonblinking behavior.

Interestingly, emission lifetimes show a similar volume thresholding behavior (Figure 4). Below a particle volume of
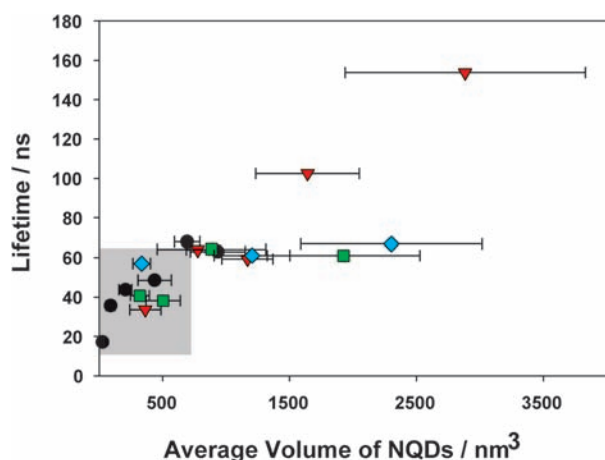

Figure 4. Average photoluminescence decay lifetime versus NQD volume as a function of starting CdSe core size: black = small core ($d = 2.2$ nm), red = medium core ($d = 3.0$ nm), green = large core ($d = 4.0$ nm), and blue = extra large core ($d = 5.5$ nm). A threshold volume is observed at ~ 750 nm^3, below which NQDs exhibit increasing lifetimes as a function of volume (shaded region), and above which lifetimes plateau for most core sizes. The 3.0 nm diameter core NQDs afford an exception, exhibiting increasing lifetimes with increasing particle volume for the entire series.

~ 750 nm^3, lifetimes range from ~ 20 to 50 ns, while above this volume, they reach ~ 65 ns. Unlike blinking suppression trends, however, lifetimes for most of the studied systems do not continue to increase with increasing volume. Rather, they plateau at ~ 65 ns. The longer lifetimes observed for thick-shell CdSe/CdS NQDs, compared to those characteristic of CdSe core-only or thin-shell systems (20–30 ns), are expected and result from the so-called quasi-type II alignment of core/shell conduction and valence bands. Specifically, the hole is energetically confined to the CdSe core, while the electronic wave function is able to delocalize into the CdS shell, leading to partial spatial separation of the carriers and, thereby, increased radiative lifetimes.[3] Delocalization of electrons into the full volume of the shell would afford increasing carrier spatial separation as shell thickness is increased and, hence, ever increasing radiative lifetimes. However, the extent of electronic delocalization is limited by, for example, Coulombic interactions between the carriers,[23] which likely results in the observed lifetime saturation. It is unclear why one core-size system (3.0 nm diameter) does not exhibit the lifetime cutoff at 750 nm^3. Future theoretical modeling and experimental explorations of the actual band alignments for each of the

core-size/shell systems are required to understand this apparent anomaly. Taken together—blinking and lifetime data as functions of volume, respectively—the relation between blinking and lifetime can be appreciated. Namely, nonblinking behavior is only observed for the CdSe/CdS core/shell systems characterized by longer lifetimes compared to their core-only or thin-shell counterparts, that is, $\geq \sim 65$ ns, but the highest nonblinking fractions are observed for the largest-volume particles, irrespective of emission lifetimes (compare Figures 3c and 4).

■ CONCLUSION

We have shown that the thick-shell approach to suppressing blinking behavior in NQDs is highly effective and can result in essentially complete suppression of blinking for our unusually rigorous interrogation times of ~ 1 h. We have also demonstrated that the utility of this approach is highly dependent on the precise method used for shell growth. We provide a new understanding of the constraining synthetic parameters for optimal monolayer-by-monolayer shell growth out to ~ 20 shell monolayers. Subtle differences in coordinating ligand and even noncoordinating solvent identities and concentrations, precursor/NQD ratios, and precursor anneal times dramatically impact particle morphology and phase, and, therefore, as we revealed, optical properties. Shape and crystal structure, combined with surface chemistry effects, also play a role in causing an unusual "solubility cycling" process, which we attribute to fluctuations in particle dipole moments over the course of the shell-addition process. When extreme, this dynamic aggregation process can produce some number of permanently attached (fused) particles. Surprisingly, elimination of the particle aggregation process by various means (extreme dilution, choosing a secondary rather than a primary amine ligand, or using an extreme excess of Cd and S precursors) affords poorly performing g-NQDs. In contrast, conditions that afford aggregation (though moderated to later stages in the shell-addition process) yield the optimally performing structures, hexagonally faceted wurtzite g-NQDs characterized by significantly suppressed blinking and high QYs in emission at thick shells (>50%; note: the origin of <unity QYs in the case of nonblinking g-NQDs is under investigation and may derive from the presence of "dark" fractions or, more likely, fluctuating PL intensities at the single-dot level). Lastly, the new synthetic protocol was used to assess the effect of core size on g-NQD properties. Blinking suppression was shown to "turn-on" at a particle volume of ~ 750 nm^3 and to subsequently trend approximately linearly with g-NQD volume. As expected, due to the quasi-Type II nature of the CdSe/CdS electronic structure (and the resulting partial spatial separation of excited-state electron−hole pairs), radiative lifetimes were found to be longer than the starting core lifetimes.[7] Interestingly, for most core sizes, lifetime values plateaued at ~ 65 ns at a particle volume of ~ 750 nm^3, though for one (3 nm core), lifetimes continued to increase. The exact relationship between radiative lifetime (and the correlated core/shell electronic structure) on the blinking process remains to be fully understood. It is clear, however, that the onset of blinking suppression in CdSe/CdS g-NQDs is associated with a longer lifetime of at least 65 ns.

ASSOCIATED CONTENT

Ⓢ Supporting Information

TEM, FTIR, and XRD data, and schematics of ligand surface packing. This material is available free of charge via the Internet at http://pubs.acs.org.

AUTHOR INFORMATION

Corresponding Author

jenn@lanl.gov

Notes

The authors declare no competing financial interest.

ACKNOWLEDGMENTS

REFERENCES

(1) Chen, Y.; Vela, J.; Htoon, H.; Casson, J. L.; Werder, D. J.; Bussian, D. A.; Klimov, V. I.; Hollingsworth, J. A. *J. Am. Chem. Soc.* **2008**, *130*, 5026.

(2) Vela, J.; Htoon, H.; Chen, Y. F.; Park, Y. S.; Ghosh, Y.; Goodwin, P. M.; Werner, J. H.; Wells, N. P.; Casson, J. L.; Hollingsworth, J. A. *J. Biophotonics* **2010**, *3*, 706.

(3) Mahler, B.; Spinicelli, P.; Buil, S.; Quelin, X.; Hermier, J. P.; Dubertret, B. *Nat. Mater.* **2008**, *7*, 659.

(4) Spinicelli, P.; Buil, S.; Quélin, X.; Mahler, B.; Dubertret, B.; Hermier, J.-P. *Phys. Rev. Lett.* **2009**, *102*, 136801.

(5) Park, Y. S.; Malko, A. V.; Vela, J.; Chen, Y.; Ghosh, Y.; Garcia-Santamaria, F.; Hollingsworth, J. A.; Klimov, V. I.; Htoon, H. *Phys. Rev. Lett.* **2011**, *106*, No. 187401.

(6) Htoon, H.; Malko, A. V.; Bussian, D.; Vela, J.; Chen, Y.; Hollingsworth, J. A.; Klimov, V. I. *Nano Lett.* **2010**, *10*, 2401.

(7) Garcia-Santamaria, F.; Chen, Y. F.; Vela, J.; Schaller, R. D.; Hollingsworth, J. A.; Klimov, V. I. *Nano Lett.* **2009**, *9*, 3482.

(8) (a) Pal, B. N.; Ghosh, Y.; Brovelli, S.; Laocharoensuk, R.; Klimov, V. I.; Hollingsworth, J. A.; Htoon, H. *Nano Lett.* **2009**, *12*, 331. (b) Kundu, J.; Ghosh, Y.; Dennis, A.; Htoon, H.; Hollingsworth, J. A. *Nano Lett.* **2012**, 10.1021/nl3008659.

(9) Li, J. J.; Wang, Y. A.; Guo, W. Z.; Keay, J. C.; Mishima, T. D.; Johnson, M. B.; Peng, X. G. *J. Am. Chem. Soc.* **2003**, *125*, 12567.

(10) Xie, R. G.; Kolb, U.; Li, J. X.; Basche, T.; Mews, A. *J. Am. Chem. Soc.* **2005**, *127*, 7480.

(11) Jones, M.; Scholes, G. D. *J. Mater. Chem.* **2010**, *20*, 3533.

(12) Tsao, J. A.; Coltrin, M. E.; Crawford, M. H.; Simmons, J. A. *Proc. IEEE* **2010**, *98*, 1162.

(13) Kudera, S.; Carbone, L.; Carlino, E.; Cingolani, R.; Cozzoli, P. D.; Manna, L. *Physica E* **2007**, *37*, 128.

(14) Peng, X. G.; Manna, L.; Yang, W. D.; Wickham, J.; Scher, E.; Kadavanich, A.; Alivisatos, A. P. *Nature* **2000**, *404*, 59.

(15) Peng, Z. A.; Peng, X. G. *J. Am. Chem. Soc.* **2002**, *124*, 3343.

(16) Rabani, E. *J. Chem. Phys.* **2001**, *115*, 1493.

(17) Shiang, J. J.; Kadavanich, A. V.; Grubbs, R. K.; Alivisatos, A. P. *J. Phys. Chem.* **1995**, *99*, 17417.

(18) Yu, J. H.; Joo, J.; Park, H. M.; Baik, S. I.; Kim, Y. W.; Kim, S. C.; Hyeon, T. *J. Am. Chem. Soc.* **2005**, *127*, 5662.

(19) Cho, K. S.; Talapin, D. V.; Gaschler, W.; Murray, C. B. *J. Am. Chem. Soc.* **2005**, *127*, 7140.

(20) Tang, Z. Y.; Kotov, N. A.; Giersig, M. *Science* **2002**, *297*, 237.

(21) Shim, M.; Guyot-Sionnest, P. *J. Chem. Phys.* **1999**, *111*, 6955.

(22) Cirillo, M.; Strubbe, F.; Neyts, K.; Hens, Z. *ACS Nano* **2011**, *5*, 1345.

(23) Brovelli, S.; Schaller, R. D.; Crooker, S. A.; Garcia-Santamaria, F.; Chen, Y.; Viswanatha, R.; Hollingsworth, J. A.; Htoon, H.; Klimov, V. I. *Nat. Commun.* **2011**, *2*, 280.